ACS EARTH AND SPACE CHEMISTRY

http://pubs.acs.org/journal/aesccq

Article

Examining Interstellar Ion-Neutral Reactions Using the Unified Reaction Valley Approach: The Case of the CCl^+ + CH_3CN Reaction

Kevin Fleming and Elfi Kraka*

Cite This: *ACS Earth Space Chem.* 2025, 9, 1837−1847

Read Online

ACCESS | Metrics & More | Article Recommendations | Supporting Information

ABSTRACT: Nitriles are a notable subset of nitrogen-bearing molecules detected within the interstellar medium (ISM). The cyano group (C≡N) enables these species to serve as potential chemical precursors for the formation of prebiotic molecules (e.g., amino acids) among other astrochemically relevant compounds. Acetonitrile, CH_3CN, is one of the simplest detected nitriles that has garnered the attention of the astrochemical community. In this study, a computational mechanistic investigation of the reaction between CH_3CN and the carbon monochloride cation, CCl^+, was conducted. One of the reaction's primary products, protonated acetylene ($C_2H_3^+$), was recently detected at the z = 0.89 molecular absorber in front of the quasar PKS 1830-211 [*Astron. Astrophys.* **2024**, *683*, A62], where CH_3CN [*Astron. Astrophys.* **2011**, *535*, A103] and HCl, the proposed chemical precursor of CCl^+ [*Astron. Astrophys.* **2019**, *629*, A128; *Astrophys. J.* **2009**, *706*, 1594], have been previously detected. This detection points to the possibility that the reaction occurs within this molecular absorber, and $C_2H_3^+$ could serve as a proxy for detecting CCl^+. The Unified Reaction Valley Approach (URVA) method, developed by our group, was utilized to acquire precise insights into the reaction's mechanism. Among other mechanistic insights, we find that the dissociation of the acetonitrile's CN bond is critical to the formation of the $C_2H_3^+$ molecular ion, whose exceptionally mobile hydrogen atoms are heavily involved in the four reaction pathways which produce the primary products of the reaction. This study demonstrates the utility of URVA for the in-depth mechanistic analysis of ion-neutral gas-phase reactions in the ISM.

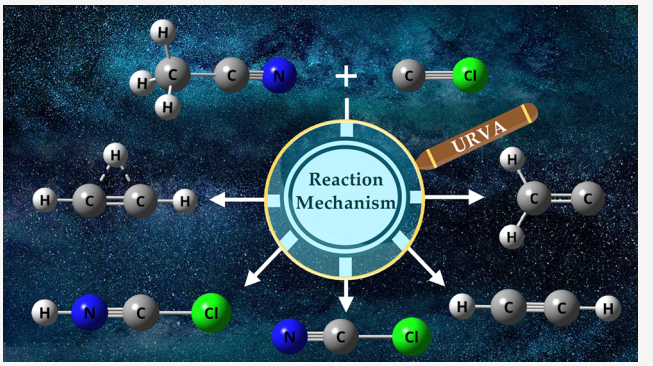

KEYWORDS: *URVA, acetonitrile, halogen, mechanistic analysis, interstellar medium, astrochemistry, ion−molecule, ion-neutral*

1. INTRODUCTION

To date, the collection of molecules detected within the interstellar medium (ISM) and circumstellar shells has grown to about 330 molecules, which are listed in the comprehensive Cologne Database for Molecular Spectroscopy (CDMS).[1−3] The experimental detection of such molecules has been facilitated by the generation of reference spectral data and the modeling of reactions between astrochemical species—these three activities together form the basis of modern-day astrochemistry.[4,5] An important subset of the detected ISM molecules are nitriles. Characterized by their cyano moiety (C≡N), these species have exceptional chemical versatility, enabling them to act as chemical precursors for various interstellar complex organic molecules (iCOMs), carbon-containing astrochemical species with six or more atoms which may have played an important role in the formation of prebiotic molecules (e.g., amino acids).[6,7] According to the exogenous hypothesis of the origin of life, extraterrestrial carriers (e.g., meteoroids and asteroids) brought prebiotic molecules to the early Earth, where they became the building blocks for the basic biomolecules of life.[8] One particular nitrile of great interest to astrochemists is acetonitrile (CH_3CN), one of the simplest nitriles reported in the CDMS. This molecule was initially detected in the Sgr A and Sgr B2 molecular clouds in 1971 through the detection of the 2.7 mm radio emission line corresponding to the nitrile's J = 6 → 5 rotational transition.[9] Since then, it has been found in comets,[10−12] star-forming regions of molecular clouds,[13−15] and protoplanetary disks,[16−18] among other sources. It is plausible that acetonitrile could either directly or indirectly serve as a chemical precursor to the formation of prebiotic compounds. For example, amino acetonitrile, which has been detected in Sgr B2(N),[19] can be formed from the photoinitiated reaction between ammonia and acetonitrile at low temperatures.[20] This derivative of acetonitrile has been proposed as a precursor for the abiotic synthesis of the fundamental prebiotic molecules glycine and adenine.[21]

Received: March 14, 2025
Revised: May 28, 2025
Accepted: June 25, 2025
Published: July 1, 2025

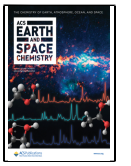

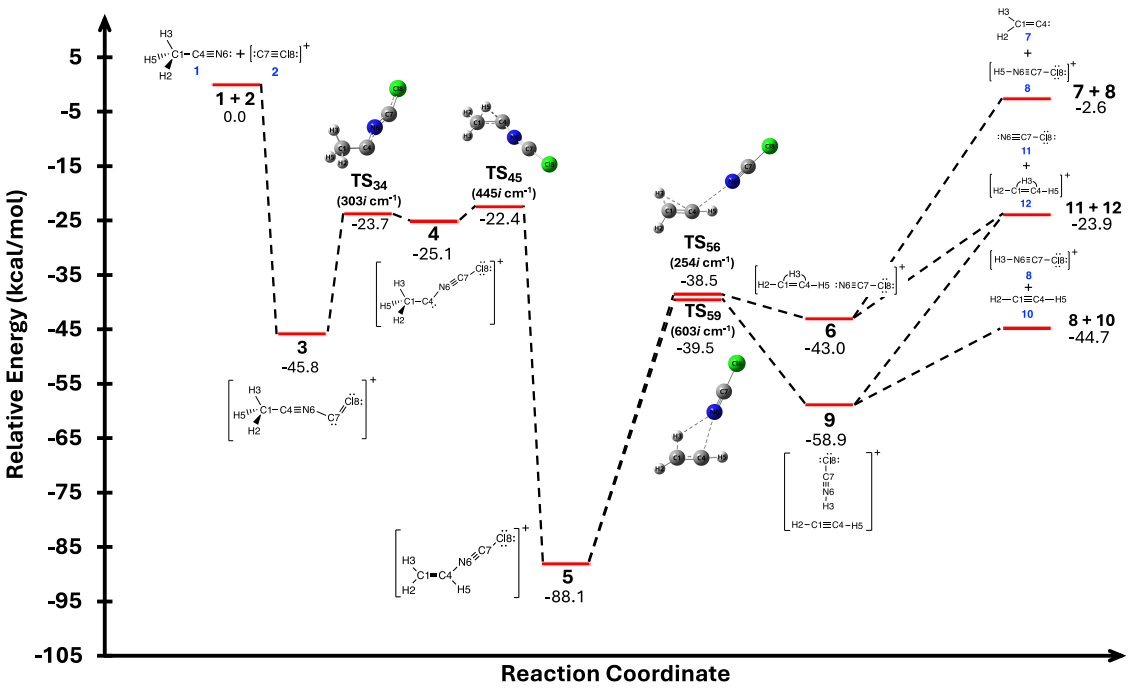

Figure 1. PES of the reaction mechanism, with ZPVE-corrected single point energies computed at the DLPNO-CCSD(T)/aug-cc-pVTZ//MP2/cc-pVTZ level of theory. All energies are reported relative to the combined single point energies of **1** and **2**. The plus signs denote infinite separation of the ion-neutral pairs. Single imaginary frequencies of transition states, computed at the MP2/cc-pVTZ level of theory, are also given.

Over the past few years, Krohn and co-workers examined various cold ion−molecule reactions in the gas phase, including those between acetonitrile and molecular ions.[22−24] The first of these studies is an investigation of the reaction between acetonitrile and the halogenated carbocation CCl^+, which is predicted to exist in the ISM but has not been detected so far.[23,25] In this study, cold CCl^+ ions were reacted with acetonitrile to produce the primary products of NCCl, $HNCCl^+$, C_2H_2, and $C_2H_3^+$.[23] One of the reaction's primary products, protonated acetylene ($C_2H_3^+$), was detected for the first time in 2024 in the z = 0.89 molecular absorber toward the quasar PKS 1830-211 using spectra obtained from the Atacama Large Millimeter/Submillimeter Array (ALMA).[26] Interestingly, CF^+, currently the only detected halogenated carbocation in the ISM, was detected there in 2016.[27] This detection of CF^+ prompts the question of whether this molecular ion's chlorinated counterpart, CCl^+, could also be detected there in the near future. Given that acetonitrile and HCl, the proposed chemical precursor of CCl^+,[25] have also been detected within the molecular absorber,[28,29] the reaction examined by Krohn and co-workers may occur there. If so, it may be possible to utilize $C_2H_3^+$ as a chemical proxy for detecting CCl^+ in future astronomical surveys. To gain further insights into this reaction, the authors also assessed microscopic kinetic rate constants through experiments and theoretical calculations, and both approaches yielded rate constants that were in good agreement with each another.[23] For the theoretical prediction of the rate constants in particular, Rice−Ramsperger−Kassel−Marcus (RRKM) theory calculations were employed.[30] The RRKM predictions were based on potential energy surface (PES) scan calculations performed by the authors to determine potential intermediates and transition states (TS) which form during the reaction.[23]

Here, beginning with the PES structures determined by Krohn and co-workers,[23] we explore the reaction between CCl^+ and CH_3CN through a unique mechanistic lens: the Unified Reaction Valley Approach (URVA), a computational method developed by our group.[31−33] Previously, we successfully utilized this method to gain detailed mechanistic insights into the gas-phase reaction between CH_4 and N^+, another ion-neutral pair, to form potentially prebiotic molecules with CN bonds in Saturn's largest moon, Titan, which is well-known for its rich atmospheric and surface chemistry.[34−38] The current study is the first application of URVA in examining ion-neutral gas-phase reactions in the ISM. We pursued the following objectives:

- to evaluate the sequence of elementary reactions which constitute the overall mechanism and to assess the energetics and thermochemistry of each elementary reaction under the conditions resembling that of the astrochemical environment in which the reacting CH_3CN and CCl^+ species may be present;
- to determine the precise sequence of bond breaking/forming and charge polarization/transfer events for each elementary reaction using URVA;
- to assess the energetic contributions of each of these mechanistic events to the overall change in the total energy of the reacting species, as well as to monitor the changes in geometry and atomic charges during each event.

2. COMPUTATIONAL METHODS

URVA was utilized in this study to assess the electronic structure changes of the reaction complex (RC), i.e., the union of the reacting species, throughout the course of the reaction mechanism.[31−33,39] For each elementary reaction of the mechanism, the RC evolves along the reaction pathway (RP) on the RC potential energy surface. The RP connects the PES stationary points associated with the reaction, which include

https://doi.org/10.1021/acsearthspacechem.5c00083
ACS Earth Space Chem. 2025, 9, 1837−1847

the local minima and, provided that the reaction is not barrierless, the intermediary TS. By evaluating the curvature of the RP for each point along the reaction coordinate, URVA allows us to pinpoint the electronic structure changes of the RC for each reaction.[31] Specifically, the curvature maxima, i.e., the curvature peaks, correspond to points along the RP where electronic structure changes indicative of important mechanistic phenomena, such as bond breaking/forming and charge polarization/transfer, occur. The curvature minima, on the other hand, are locations along the RP corresponding to minimal electronic structure changes. With this in mind, one can define a *reaction phase*, a segment of the RP for a given elementary step with two end points corresponding to curvature minima and a single intermediary point corresponding to a curvature peak.[40,41] Thus, each reaction phase represents a set of electronic structure changes to the RC. Furthermore, the individual electronic structure changes which constitute this set can be determined by the decomposition of the overall curvature into individual curvature components due to the changes in the RC's geometric parameters, such as bond lengths, bond angles, dihedral angles,[42] or other coordinates of choice including, e.g., Cremer−Pople puckering coordinates.[43] When a curvature component is negative or positive for a given curvature peak, the parameter associated with that curvature component either resists or supports the chemical change associated with that curvature peak, respectively.[42] Therefore, dividing the RP curvature profile of each elementary step into a series of successive reaction phases, followed by the decomposition of the overall curvature into its constituent components for each reaction phase, enables the precise evaluation of the sequence of electronic structure changes which characterizes that step.[31,32] Our group has applied URVA to a wide variety of chemical reactions, ranging from those involving small organic molecules—in different environments such as gas phase, solution, and/or in enzymes—to those involving large organometallic complexes; we have published a comprehensive review of these works,[31] as well as a detailed description of the mathematical formalism of URVA.[32]

Geometry optimization and frequency calculations of the stationary points, shown in Figure 1, were performed with second-order Møller−Plesset perturbation theory (MP2)[44,45] and the Dunning cc-pVTZ[46,47] basis set. The initial geometries of the stationary points—with the exception of $\mathbf{TS_{34}}$ and intermediate **4**—were previously determined and optimized by Krohn and co-workers at the M06-2X[48]/aug-cc-pVTZ[47,49] and MP2/aug-cc-pVTZ levels of theory, respectively.[23] Single point energies of the reoptimized geometries were computed at the domain-based local pair natural orbital coupled-cluster theory (DLPNO-CCSD(T))[50]/aug-cc-pVTZ level of theory using ORCA 5.0.4., with an self-consistent field (SCF) convergence threshold of 10^{-9} E_h between successive cycles.[51] Zero-point vibrational energy (ZPVE) corrections obtained from the frequency calculations were applied to these single point energies. The frequency calculations also yielded the reaction enthalpies and Gibbs free energies of the elementary reactions **R1**−**R9** shown in Figure 1, as well as the activation enthalpies and Gibbs free energies of **R2**, **R3**, **R4**, and **R7**, all of which were recomputed for a temperature of 10 K and a concentration of 2.4908×10^{-19} mol/L (~150 molecules/cm^3) using the GoodVibes thermochemistry program[52] to represent the conditions of diffuse molecular clouds where acetonitrile has been detected, such as Sg B2.[9,53,54] Reaction path calculations were performed at the MP2/cc-pVTZ level of theory, and the Intrinsic Reaction Coordinate (IRC) method[55] was applied with a step size of $s = 0.03$ amu$^{1/2}$ bohr. All of the geometry optimization, frequency, and IRC calculations were run on Gaussian 16.[56] All Gaussian calculations utilized the default `UltraFine` integration grid, consisting of 99 radial shells and 590 angular points per shell; the default geometry optimization convergence thresholds utilized are the following: 0.0003 E_h/bohr (root mean square force), 0.00045 E_h/bohr (maximum force), 0.0012 E_h/rad (root mean square displacement), and 0.0018 E_h/rad (maximum displacement).[56] The RC's atomic charges and Lewis structures were evaluated with the natural bond orbital (NBO) analysis method.[57] URVA analysis was performed for **R1**−**R9** with the pURVA program.[58] To facilitate URVA calculations, all preceding IRC calculations implemented the improved reaction path following procedure of Hratchian and Kraka for tracking each elementary reaction far out into its specific entrance and exit channels.[59]

3. RESULTS AND DISCUSSION

3.1. Reaction Mechanism and Energetics. Figure 1 depicts the sequence of elementary reactions responsible for the transformation of reactants **1** and **2** to products **7**, **8**, **10**, **11**, and **12**, as well as the three-dimensional (3D) geometries of transition states $\mathbf{TS_{34}}$, $\mathbf{TS_{45}}$, $\mathbf{TS_{56}}$, and $\mathbf{TS_{59}}$. The reaction and activation energies of each reaction were computed at the DLPNO-CCSD(T)/aug-cc-pVTZ//MP2/cc-pVTZ level of theory, and they are listed in Table 1. Due to the low temperature and pressure conditions considered, the reaction and activation energies are very similar to the corresponding reaction/activation enthalpies and free energies for each reaction (with the greatest observed difference of ~1 kcal/mol for the barrierless association/dissociation reactions due to their non-negligible entropic changes; see Supporting Information). The following discussion will therefore be focused on the energetics of the reactions.

Table 1. Activation Energies (E^a) and Reaction Energies (E_r) of Reactions R1−R9, Computed at the DLPNO-CCSD(T)/aug-cc-pVTZ//MP2/cc-pVTZ Level of Theory[a]

reaction	E^a	E_r
R1 (**1** + **2** → **3**)		−45.8
R2 (**3** → **4**)	22.1	20.7
R3 (**4** → **5**)	2.7	−63.0
R4 (**5** → **6**)	49.6	45.1
R5 (**6** → **7** + **8**)		40.4
R6 (**6** → **11** + **12**)		19.1
R7 (**5** → **9**)	48.6	29.2
R8 (**9** → **11** + **12**)		35.0
R9 (**9** → **8** + **10**)		14.1

[a]Activation energies are reported only for **R2**, **R3**, **R4**, and **R7**, as these are the only reactions with activation barriers. All values are reported in kcal/mol.

Reaction **R1** is described by the approach and unification of the reacting acetonitrile (**1**) and carbon monochloride cation (**2**) species to form intermediate **3**. This barrierless reaction is highly exothermic, and the endothermic reaction **R2** utilizes a fraction of the energy released from **R1** to force **3** to overcome an activation barrier of 22.5 kcal/mol and transform into the unstable carbene **4**. Intermediate **4**, the most unstable

https://doi.org/10.1021/acsearthspacechem.5c00083
ACS Earth Space Chem. 2025, 9, 1837−1847

intermediate on the RC PES, undergoes the hydrogen migration reaction **R3** to convert into **5**, the most stable intermediate on the PES (Figure 1). Consequently, **R3** is highly exothermic; it is also kinetically favorable due to the low activation energy barrier of 2.7 kcal/mol. The energy released from reaction **R3**, combined with the unspent energy released from reaction **R1**, is approximately sufficient for **5** to take one of four reaction pathways shown in Figure 1: path 1a (**R4** → **R5**), path 1b (**R4** → **R6**), path 2a (**R7** → **R8**), and path 2b (**R7** → **R9**). Comparing the energetic requirements of the four paths, however, it is clear that path 1b and path 2b are less energetically demanding and therefore more favorable than path 1a and path 2a.

Both path 1a and path 1b begin with reaction **R4**, which involves the dissociation of **5**'s CN single bond, as well as the formation of a nonclassical three-center, two-electron (3c−2e) bond involving one of its terminal hydrogen atoms, to form two interacting molecular fragments which constitute intermediate **6**. In sharp contrast to the preceding **R3** reaction, **R4** is the most endothermic step in the overall mechanism. Furthermore, this reaction's high activation barrier of 49.6 kcal/mol positions it to be the least kinetically favorable reaction in the overall mechanism. Intermediate **6**, once formed, is the point at which path 1a and path 1b diverge on the RC PES. In the case of path 1a, a hydrogen atom is transferred between the two molecular fragments of **6** during barrierless reaction **R5** to yield products **7** and **8**. Path 1b, in contrast, simply involves the gradual dissociation of the two fragments to form the corresponding products **11** and **12** by the barrierless reaction **R6**. Consequently, although **R5** and **R6** are both endothermic, there is an approximate factor-of-two difference between their reaction energies of 40.4 and 19.1 kcal/mol, respectively, indicating that path 1b is ultimately a significantly more favorable reaction path for intermediate **6**.

Reaction **R7**, like reaction **R4**, also involves the dissociation of the CN single bond of **5**, but the former differs from that latter in that it involves the subsequent dissociation of a terminal CH single bond and the formation of a terminal NH single bond to form two interacting molecular fragments which constitute intermediate **9**. **R7** is the starting point for both path 2a and path 2b, and the resulting intermediate **9** acts as the point along the RC PES at which the two paths diverge. In path 2a, **9** undergoes the barrierless hydrogen transfer reaction **R8**, akin to **R5** of path 1a, to generate products **11** and **12**, the same set of products observed for reaction **R6** of path 1b. Path 2b involves the gradual dissociation of the two molecular fragments of **9** via barrierless reaction **R9**, akin to **R6**, to form the corresponding products **8** and **10**. Given these parallels between **R5** and **R8**, as well as those between **R6** and **R9**, it is perhaps not surprising that, similar to the factor-of-two difference in reaction energies for **R5** and **R6**, an approximate factor-of-two difference in the reaction energies of **R8** and **R9** (35.0 and 14.1 kcal/mol, respectively) is observed. Thus, as observed for path 1b when compared to path 1a, path 2b is considerably more energetically favorable than path 2a for intermediate **9**.

While most of the mechanistic structures' geometries, which were computed at the MP2/cc-pVTZ level of theory, are similar to those computed by Krohn and co-workers at the MP2/aug-cc-pVTZ level of theory, a few notable differences are present. First, for the isomerization reaction **R2**, relaxed PES scans revealed a transition state, TS_{34}, which transforms into the metastable intermediate **4** located in a very shallow well on the PES, shown in Figure 1. These two structures were previously unreported, although the authors did note that a shallow well between INT1 and TS1, two PES structures they found during their PES scan (analogous to **3** and TS_{45}, respectively), may be present based on one's choice of the level of theory.[23] Furthermore, intermediate **6** differs from an analogous intermediate structure reported by the authors, INT3.[23] More specifically, the $C_2H_3^+$ fragment in **6** adopts a nonclassical bridged geometry, with atom H3 situated right above the center of the fragment's C1C4 bond, while INT3 adopts the classical Y-shaped geometry of protonated acetylene.[23] Previous quantum chemical calculations[60−65] and experimental investigations[66−69] have confirmed that that the bridged isomer of protonated acetylene is more energetic stable (by ∼4 kcal/mol) than its Y-shaped counterpart, with a small energetic barrier to go from the latter to the former (≤1 kcal/mol). Lastly, since the protonated acetylene fragment of intermediate **6** is in the bridged isomeric form, the two fragments of the intermediate's van der Waals (VdW) complex can readily undergo dissociation to form products **11** and **12**, which are also produced via reaction **R8**. We find, therefore, that there are two elementary reactions that can produce bridged, protonated acetylene (**R6** and **R8**), just as there are two elementary reactions to form the $HNCCl^+$ product (**R5** and **R9**), as shown in Figure 1. The similarity between the reaction energies of **R5** and **R8**, as well as those of **R6** and **R9** (Table 1), indicates that kinetic modeling of the overall reaction based on the PES shown in Figure 1 would yield a theoretical $HNCCl^+$ to $C_2H_3^+$ branching ratio that should be in good agreement with the experimentally determined branching ratio of approximately 50:50;[23] for this study, however, we did not conduct such modeling.

To complement our calculations of the energetics of reactions **R1**−**R9**, a detailed mechanistic analysis of each elementary step was also conducted. Since energy is a cumulative property of the RC,[41] it cannot be used to provide a detailed description of the sequence of mechanistic events which characterizes each elementary reaction. To address this, a discussion of the URVA results will be presented.

3.2. URVA Description of Reaction Mechanism. The URVA results for **R1**−**R9** were examined by evaluating the following for each phase of each reaction as a function of the reaction parameter *s*: the changes to RC energy, the changes in NBO atomic charges, the changes in the RP curvature along with its decomposition into relevant curvature components, and the changes in the geometric parameters associated with each of these curvature components. By piecing together these complementary data sets, a precise description of the evolution of the RC for a given elementary reaction can be acquired. Detailed phase-by-phase descriptions for all elementary reactions, with the exception of **R6** and **R9**, which involve only the dissociation of their respective VdW complexes, are provided in the Supporting Information. Reaction animations showing the geometric changes of the RC for **R1**−**R9**, as well as the associated geometries for all stationary points/TS/VdW complexes, can also be found in the Supporting Information. The detailed mechanistic descriptions of the nine elementary reactions allowed us to categorize the reactions based on their roles in the transformation of the RC from the reactants to the experimentally observed products, as described below.

*3.2.1. Formation, Destabilization, and Subsequent Stabilization of the RC (**R1**−**R3**).* Intermediate **3**, formed from the union of reactants **1** and **2** during synthesis reaction

https://doi.org/10.1021/acsearthspacechem.5c00083
ACS Earth Space Chem. 2025, 9, 1837−1847

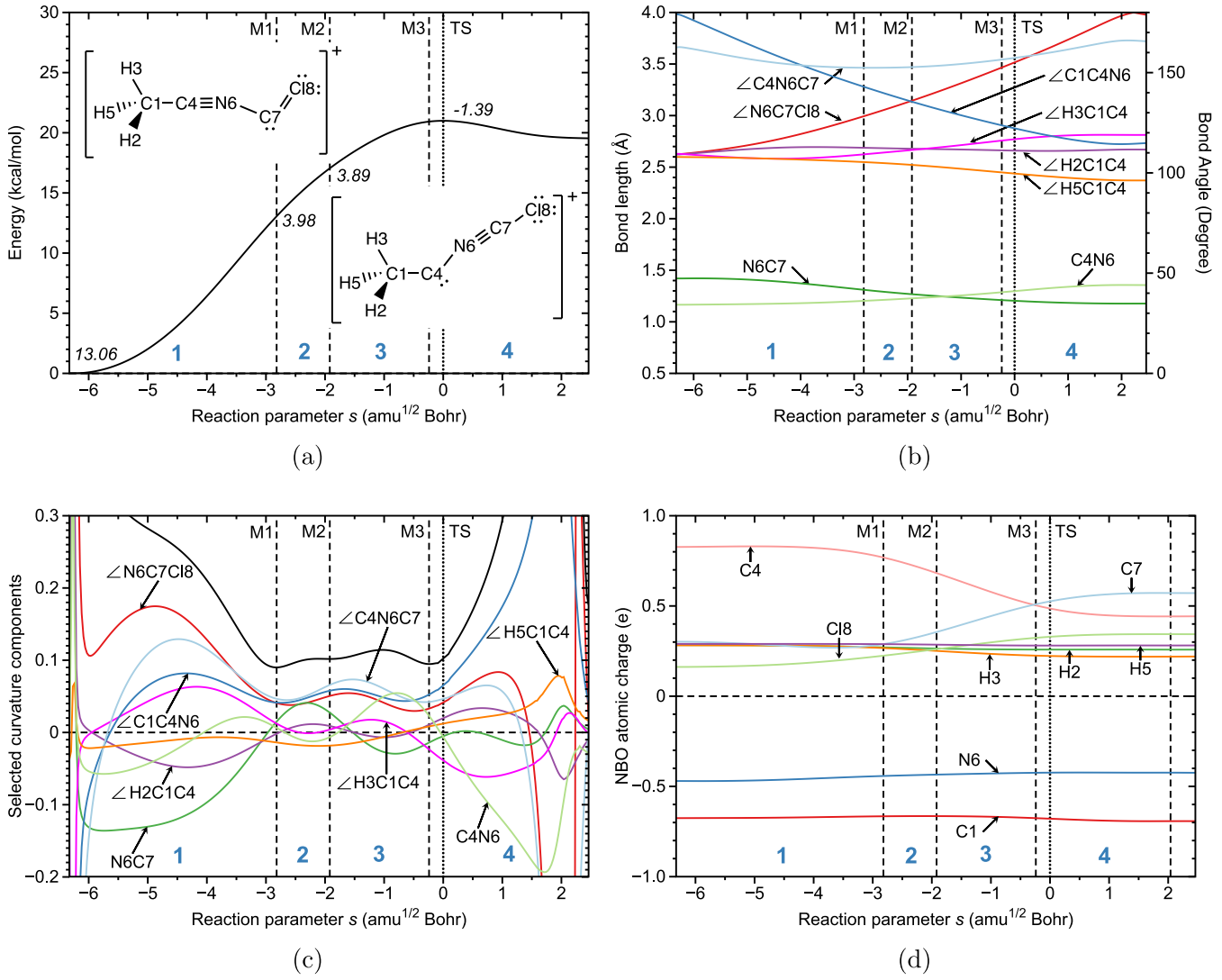

Figure 2. Evolution of the RC in reaction **R2** as a function of reaction parameter *s*, as illustrated by the (a) reaction energy profile (with RC energy changes for each phase), (b) changes in RC geometric parameters, (c) total RP curvature (solid black line) and corresponding curvature components (colored solid lines), and (d) changes in NBO atomic charges. Curvature minima are denoted by black dotted lines M1−M3, while TS is denoted by the black dotted line at $s = 0$ amu$^{1/2}$ bohr. Reaction phases 1−4 are shown above for each plot. MP2/cc-pVTZ level of theory.

R1, endothermically isomerizes in four-phase reaction **R2**, shown in Figure 2, to form highly unstable carbene intermediate **4**. The first of these four phases, which is also the most energetically demanding phase, involves significant conformational changes to the bond angles involving atoms C4, N6, C7, and C8, indicative of the start of the change in the hybridization of atoms C4 (sp to sp^2) and C7 (sp^2 to sp). This switch in the hybridization of the two carbons reflects the drastic switch in the bond orders of the C4N6 and C7N6 bonds, with the former reduced to a single bond and the latter promoted to a triple bond. Phases 2 and 3 describe the intermediate steps of this process, during which intermediate **3** converts into a transient ylide in which both CN bonds are double bonds. Soon thereafter, the ylide converts into the previously unreported late transition state $\mathbf{TS_{34}}$, which undergoes further conformational changes during phase 4 to yield metastable carbene intermediate **4**. Although the cyano group of the acetonitrile reactant contributes to the formation of the RC in reaction **R1** via the formation of a CN bond with the electrophilic CCl^+ species, in reaction **R2**, it contributes to the destabilization of the RC through the formation of the carbene. However, this destabilization serves a critical role in the mechanism. During reaction **R3**, the carbene, the most unstable intermediate in the mechanism, exothermically converts to **5**, the most stable intermediate in the overall mechanism. In this three-phase process, shown in Figure 3, the hydrogen atom H5 migrates to the highly nucleophilic carbenoid atom C4 to form **5**. During phase 1, H5 promptly begins migrating toward C4, yielding the early transition state $\mathbf{TS_{45}}$. Concurrently, the electron density responsible for the C1H5 bond begins to shift toward C4, resulting in the formation of a transient 3c−2e bond between H5, C1, and C4 during phase 2. This nonclassical bond quickly dissociates, resulting in the formation of a C1C4 double bond, while H5 goes on to form a single bond with C4 during phase 3 to yield intermediate **5**.

*3.2.2. Dissociation of the Stabilized RC—Paths 1a and 1b (**R4**−**R6**).* Reaction **R4**, the first reaction for both path 1a and path 1b, involves the splitting of intermediate **5** into two noncovalently bound fragments, which subsequently undergoes rearrangement to form the intermediate VdW complex **6**. This elementary reaction, an endothermic, eight-phase process

https://doi.org/10.1021/acsearthspacechem.5c00083
ACS Earth Space Chem. 2025, 9, 1837−1847

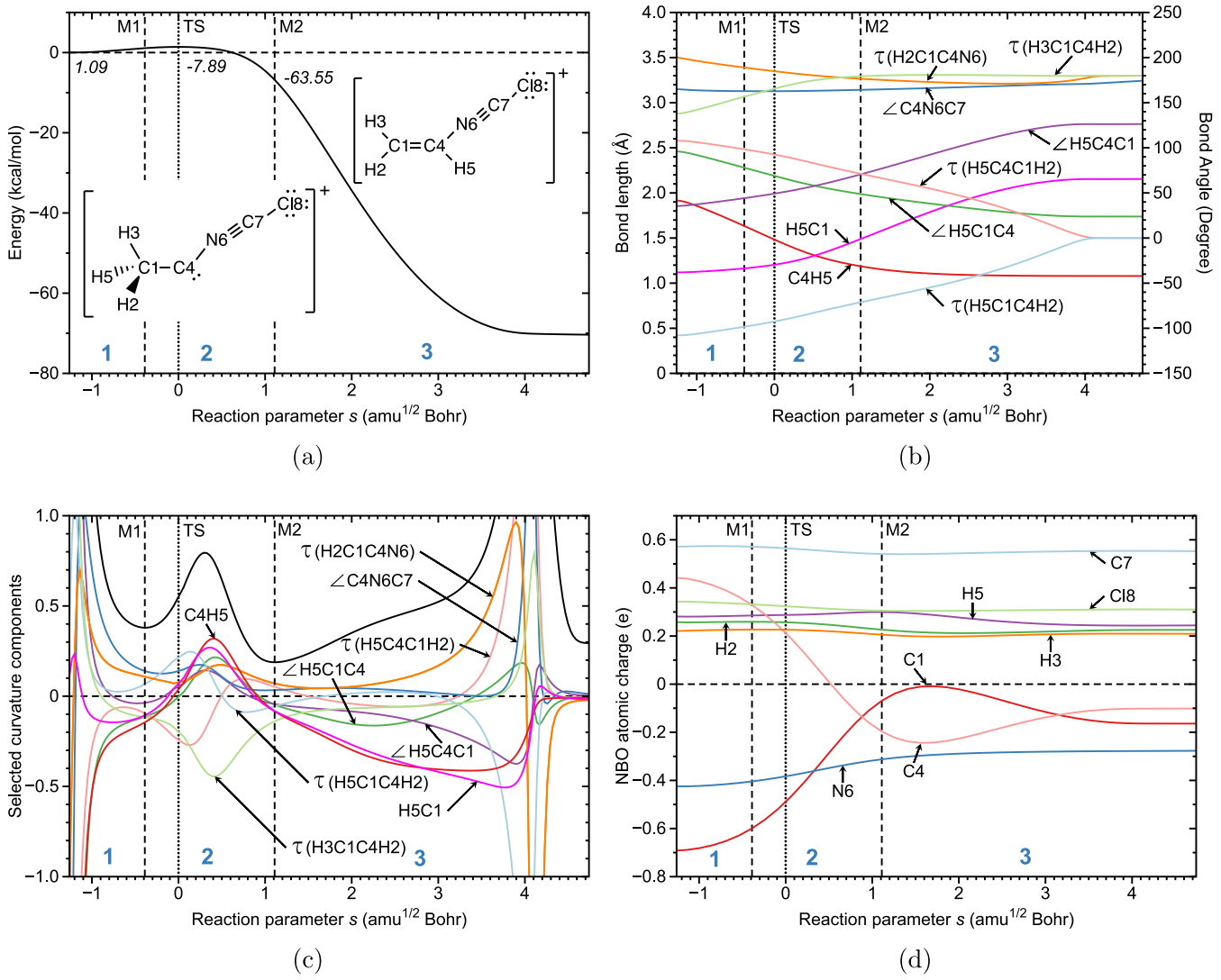

Figure 3. Evolution of the RC in reaction **R3** as a function of reaction parameter *s*, as illustrated by the (a) reaction energy profile (with RC energy changes for each phase), (b) changes in RC geometric parameters, (c) total RP curvature (solid black line) and corresponding curvature components (colored solid lines), and (d) changes in NBO atomic charges. Curvature minima are denoted by black dotted lines M1 and M2, while TS is denoted by the black dotted line at s = 0 amu$^{1/2}$ bohr. Reaction phases 1−3 are shown above for each plot. MP2/cc-pVTZ level of theory.

shown in Figure 4, involves several bond-breaking/bond-forming processes, which result in an atypical reaction energy profile. Phases 1 and 2 describe the energetically demanding cleavage of the C4N6 bond of **5** to form a VdW complex with $C_2H_3^+$ and NCCl fragments. After the dissociation of the bond, the H2 atom of the $C_2H_3^+$ fragment begins migrating toward the carbon atom C4. This process begins in phase 2 and ends in phase 4, when it results in the formation of a transient 3c−2e bond involving atoms H2, C1, and C4. The nonclassical bond dissociates as soon as it is formed, forcing atom H2 to return back to C1. This sudden change causes a sharp jump in the energy of the RC during phase 5, leading to $\mathbf{TS_{56}}$, which has a $C_2H_3^+$ fragment resembling the classical Y-shaped isomer of protonated acetylene. In phases 6 and 7, this classical structure isomerizes to the lower-energy nonclassical bridged structure due to the migration of H3 toward atom C4, which results in a new 3c−2e bond involving atoms H3, C1, and C4 by the end of phase 7. The interconversion between the nonclassical and classical forms of the $C_2H_3^+$ fragment results in the anomalous shape of the energy profile during phases 4−7. Both the $C_2H_3^+$ and NCCl fragments complete their reorientation in phase 8 to yield the VdW complex given by intermediate **6**. This intermediate can evolve in one of two ways. The first option, where it undergoes proton transfer between its two fragments (followed by the dissociation of the fragments), occurs via the seven-phase barrierless reaction **R5** of path 1a to yield products **7** and **8**; in the second option, **6** can undergo less energetically demanding dissociation by the separation of its two fragments via barrierless reaction **R6** of path 1b to yield products **11** and **12**.

*3.2.3. Dissociation of the Stabilized RC—Paths 2a and 2b (**R7**−**R9**).* Reaction **R7**, the first reaction for both path 2a and path 2b, involves the splitting of intermediate **5** into two noncovalently bound fragments, which subsequently undergoes rearrangement to form the intermediate VdW complex **9**. Like reaction **R4**, this elementary step also has an unusual energy profile, which can be understood by examining its seven reaction phases, shown in Figure 5. Phases 1 and 2, akin to their counterparts for **R4**, also describe the dissociation of the C4N6 bond in **5** to form a VdW complex involving $C_2H_3^+$ and NCCl fragments. Soon after this dissociation step, the hydrogen atom H3 begins migrating toward the now-

https://doi.org/10.1021/acsearthspacechem.5c00083
ACS Earth Space Chem. 2025, 9, 1837−1847

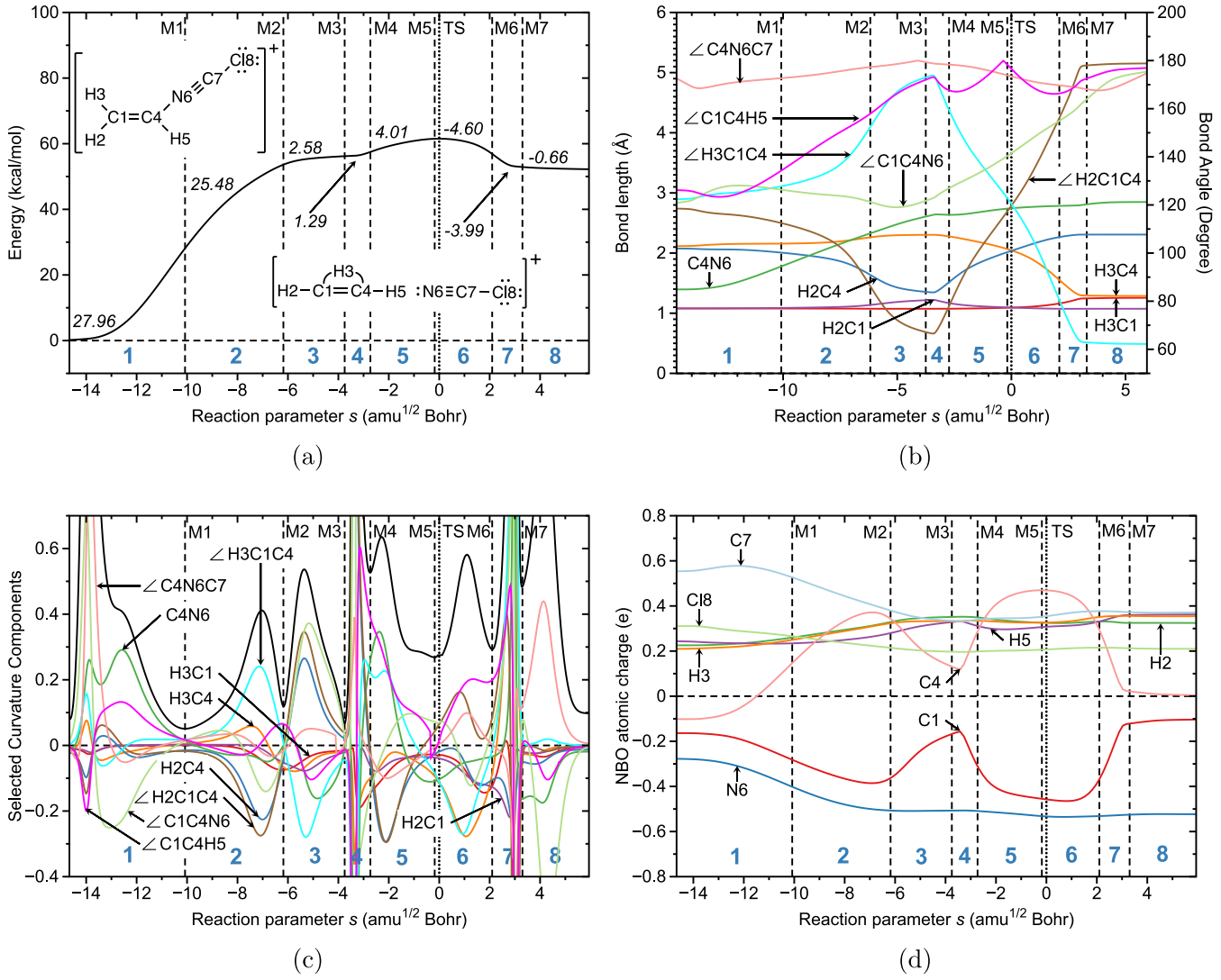

Figure 4. Evolution of the RC in reaction **R4** as a function of reaction parameter *s*, as illustrated by the (a) reaction energy profile (with RC energy changes for each phase), (b) changes in RC geometric parameters, (c) total RP curvature (solid black line) and corresponding curvature components (colored solid lines), and (d) changes in NBO atomic charges. Curvature minima are denoted by black dotted lines M1−M7, while TS is denoted by the black dotted line at s = 0 amu$^{1/2}$ bohr. Reaction phases 1−8 are shown above for each plot. MP2/cc-pVTZ level of theory.

electron-deficient C4 atom, which culminates in the formation of a transient 3c−2e bond between H3, C1, and C4 during phase 3. At the beginning of phase 4, this bond dissociates, resulting in the formation of a triple bond between atoms C1 and C4, converting the protonated acetylene fragment into neutral acetylene. For the remainder of this phase, the liberated H3 atom migrates to the NCCl fragment as the C_{2v} symmetric T-structure of intermediate **9** begins to form, resulting in the observed shoulder in the energy profile during this phase. During phase 5, the H3 atom binds to atom N6 of the NCCl fragment, resulting in a new, linear $HNCCl^+$ fragment, which is reorientated during phases 6 and 7 such that it is perpendicular to the acetylene fragment to yield intermediate **9**, which can be described as π-complex with electron density present along its C_2 axis.[70] This intermediate can evolve in one of two ways. The first option, where it undergoes proton transfer between its two fragments (followed by the dissociation of the fragments), occurs via the seven-phase barrierless reaction **R8** of path 2a to yield products **11** and **12**; in the second option, **9** can undergo less energetically demanding dissociation by the separation of its two fragments via the barrierless reaction **R9** of path 2b to yield products **8** and **10**.

4. CONCLUSIONS

The mechanistic analysis of this reaction ultimately answers a question posed by Krohn and co-workers in their study:[23] does the formation of the experimentally observed products require the cleavage of acetonitrile's CN bond, and if so, why? Our findings suggest that the dissociation of acetonitrile's CN bond in reactions **R4** and **R7** is necessary, since the dissociation results in the creation of a $C_2H_3^+$ molecular ion, transient or otherwise, which is necessary for the four aforementioned reaction pathways following intermediate **5**. The high flexibility and mobility of the ion's hydrogen atoms, which we observed from the URVA results and the reaction animations, enable the formation of the diverse set of experimentally observed products, each of which are made up of various combinations of H, N, C, and Cl atoms. The migration of the ion's hydrogen atoms can also be induced through its exposure to electromagnetic radiation, which pervades the ISM. In previous work

https://doi.org/10.1021/acsearthspacechem.5c00083
ACS Earth Space Chem. 2025, 9, 1837−1847

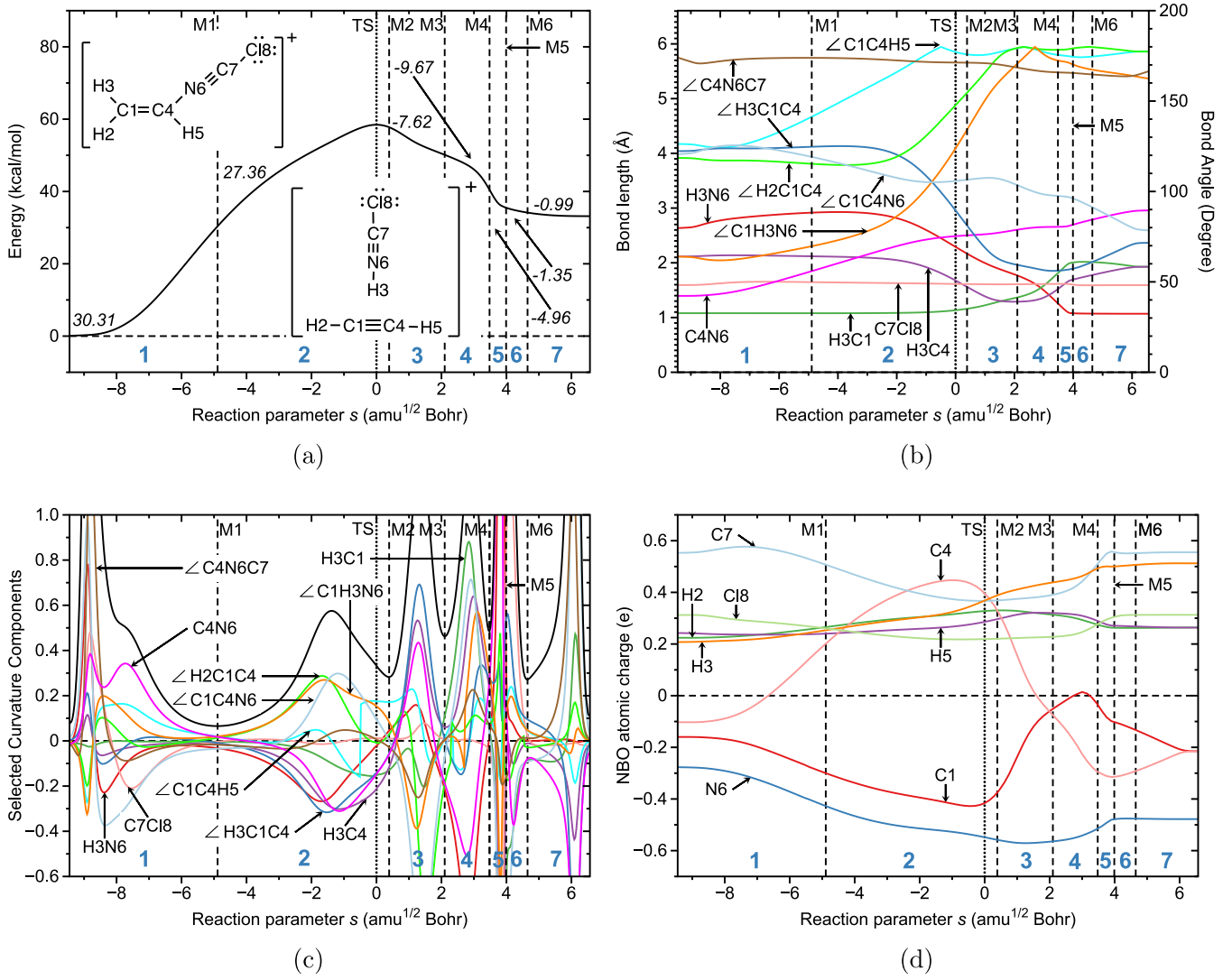

Figure 5. Evolution of the RC in reaction **R7** as a function of reaction parameter *s*, as illustrated by the (a) reaction energy profile (with RC energy changes for each phase), (b) changes in RC geometric parameters, (c) total RP curvature (solid black line) and corresponding curvature components (colored solid lines), and (d) changes in NBO atomic charges. Curvature minima are denoted by black dotted lines M1−M6, while TS is denoted by the black dotted line at s = 0 amu$^{1/2}$ bohr. Reaction phases 1−7 are shown above for each plot. MP2/cc-pVTZ level of theory.

conducted by Shi and co-workers, Born−Oppenheimer molecular dynamics simulations were utilized to demonstrate that these hydrogens, when exposed to high-frequency, circularly polarized light, can migrate around the two central carbon atoms (i.e., a propeller-like motion), causing the ion to alternate between the aforementioned bridged and Y-shaped isomers on the ion's PES[71]—similar to the chemically induced interconversion between the two isomers observed in reaction **R4**. Interestingly, significant amounts of high-frequency circularly polarized light have been observed in star-forming regions of the ISM,[72] so the chemistry of the newly detected $C_2H_3^+$ ion in molecular clouds may be influenced by reactions with other astrochemical species as well as its interactions with the circularly polarized light that may be emitted from the star-forming cores of molecular clouds. This exceptional chemical versatility of $C_2H_3^+$ may pave the way for a rich interstellar chemistry, especially considering that this ion can also undergo an electron recombination reaction to form the acetylene molecule, which has been extensively investigated for its role in the evolution of chemical complexity in the ISM, including the formation of polycyclic aromatic hydrocarbon compounds and other iCOMs of astrochemical/astrobiological relevance.[73] Thus, the interstellar chemistry of this ion, particularly with respect to the formation of iCOMs through gas-phase ion-neutral reactions, merits further investigation. This work demonstrates, as a proof of concept, the utility of URVA as an effective computational tool for such a potential future research endeavor.

Our findings also prompt the question of whether the CN bond dissociation observed in this study can be expected for all nitriles in the ISM. The nucleophilicity of the terminal nitrogen on acetonitrile enabled it to react with the electrophilic carbon of the CCl^+ species. Beginning from reaction **R1**, electron density was gradually transferred from acetonitrile's CN bond to the newly formed CN bond during the formation, destabilization, and subsequent stabilization of the RC, resulting in the transformation of acetonitrile's strong CN triple bond to a weak single bond susceptible to cleavage (and vice versa for the adjacent CN bond) by the end of reaction **R3**. To break one strong CN bond, another strong CN bond had to be made. However, dissociation may have not occurred if the CN bond was bound to a strong electron-withdrawing

https://doi.org/10.1021/acsearthspacechem.5c00083
ACS Earth Space Chem. 2025, 9, 1837−1847

group instead of the electron-donating methyl group of acetonitrile. A strong electron-withdrawing group potentially could withdraw significant electron density from the CN bond, thereby partially or entirely deactivating the bond and rendering it be less reactive or even unreactive when it encounters the CCl^+ species. One class of interstellar nitriles for which CN deactivation could occur are cyanopolyynes. Cyanoacetylene (HC_2CN), the smallest detected cyanopolyyne detected in the ISM,[74] has an unsaturated, electron-withdrawing ethynyl group attached to its CN bond, which may render the terminal nitrogen to be less nucleophilic and prevent the CN bond from undergoing cleavage if one attempted to react the molecule with CCl^+. The larger cyanopolyynes may exhibit a similar behavior since they have even longer chains of relatively electronegative sp-hybridized carbons bound to the CN bond. On the contrary, if nitriles with electron-donating groups are considered, CN bond dissociation may be more likely to occur. Examples of these nitriles include other detected alkylated nitriles besides acetonitrile, such as ethyl cyanide[75] and propyl cyanide.[76] Future mechanistic studies utilizing URVA alongside kinetic modeling could evaluate the extent to which electron-donating/-withdrawing functional groups influence the cleavage of a given nitrile's CN bond during reactions with halogenated carbocations such as CCl^+ and its detected, fluorinated counterpart CF^+.[77]

■ ASSOCIATED CONTENT

Supporting Information

The Supporting Information is available free of charge at https://pubs.acs.org/doi/10.1021/acsearthspacechem.5c00083.

Energetics and thermochemistry of reactions **R1**−**R9** at DLPNO-CCSD(T)/aug-cc-pVTZ//MP2/cc-pVTZ level of theory, MP2/cc-pVTZ geometries of stationary points/TS/VdW complexes of reactant/product structures, and detailed URVA phase analysis of elementary reactions (PDF)

Reaction animations of **R1**−**R9** (MP4 files) (ZIP)

■ AUTHOR INFORMATION

Corresponding Author

Elfi Kraka − *Computational and Theoretical Chemistry Group (CATCO), Department of Chemistry, Southern Methodist University, Dallas, Texas 75275-0314, United States;* orcid.org/0000-0002-9658-5626; Email: ekraka@mail.smu.edu

Author

Kevin Fleming − *Computational and Theoretical Chemistry Group (CATCO), Department of Chemistry, Southern Methodist University, Dallas, Texas 75275-0314, United States*

Complete contact information is available at: https://pubs.acs.org/10.1021/acsearthspacechem.5c00083

Notes

The authors declare no competing financial interest.

■ ACKNOWLEDGMENTS

This work was financially supported by the National Science Foundation, Grant CHE 2102461. We thank Dr. Marek Freindorf for his valuable suggestions during this study. In addition, we would also like to thank the SMU O'Donnell Data Science and Computing Center for providing excellent computational resources and the SMU Moody School of Graduate and Advanced Studies for supporting this work through the SMU Moody Graduate Fellowship.

■ REFERENCES

(1) Endres, C. P.; Schlemmer, S.; Schilke, P.; Stutzki, J.; Müller, H. S. The Cologne Database for Molecular Spectroscopy, CDMS, in the Virtual Atomic and Molecular Data Centre, VAMDC. *J. Mol. Spectrosc.* **2016**, *327*, 95−104.

(2) Müller, H. S.; Schlöder, F.; Stutzki, J.; Winnewisser, G. The Cologne Database for Molecular Spectroscopy, CDMS: a useful tool for astronomers and spectroscopists. *J. Mol. Struct.* **2005**, *742*, 215−227.

(3) Müller, H. S. P.; Thorwirth, S.; Roth, D.; Winnewisser, G. The Cologne database for molecular spectroscopy, CDMS. *A&A* **2001**, *370*, L49−L52.

(4) Fortenberry, R. C. A Vision for the Future of Astrochemistry in the Interstellar Medium by 2050. *ACS Phys. Chem. Au* **2024**, *4*, 31−39.

(5) Fortenberry, R. C. Quantum Chemistry and Astrochemistry: A Match Made in the Heavens. *J. Phys. Chem. A* **2024**, *128*, 1555−1565.

(6) Herbst, E.; Van Dishoeck, E. F. Complex Organic Interstellar Molecules. *Annu. Rev. Astron. Astrophys.* **2009**, *47*, 427−480.

(7) Ceccarelli, C.; Caselli, P.; Fontani, F.; Neri, R.; López-Sepulcre, A.; Codella, C.; Feng, S.; Jiménez-Serra, I.; Lefloch, B.; Pineda, J.; et al. Seeds of Life in Space (SOLIS): The Organic Composition Diversity at 300−1000 AU Scale in Solar-Type Star-Forming Regions. *Astrophys. J.* **2017**, *850*, 176.

(8) Ruiz-Mirazo, K.; Briones, C.; de la Escosura, A. Prebiotic Systems Chemistry: New Perspectives for the Origins of Life. *Chem. Rev.* **2014**, *114*, 285−366.

(9) Solomon, P. M.; Jefferts, K.; Penzias, A.; Wilson, R. Detection of Millimeter Emission Lines from Interstellar Methyl Cyanide. *Astrophys. J.* **1971**, *168*, L107.

(10) Hänni, N.; Altwegg, K.; Balsiger, H.; Combi, M.; Fuselier, S.; De Keyser, J.; Pestoni, B.; Rubin, M.; Wampfler, S. Cyanogen, Cyanoacetylene, and Acetonitrile in Comet 67P and Their Relation to the Cyano Radical. *Astron. Astrophys.* **2021**, *647*, No. A22.

(11) Kissel, J.; Krueger, F. The Organic Component in Dust from Comet Halley as Measured by the PUMA Mass Spectrometer on Board Vega 1. *Nature* **1987**, *326*, 755−760.

(12) Biver, N.; Bockelee-Morvan, D.; Colom, P.; Crovisier, J.; Davies, J. K.; Dent, W. R.; Despois, D.; Gerard, E.; Lellouch, E.; Rauer, H.; et al. Evolution of the Outgassing of Comet Hale-Bopp (C/1995 O1) From Radio Observations. *Science* **1997**, *275*, 1915−1918.

(13) Hsieh, T.-H.; Segura-Cox, D.; Pineda, J.; Caselli, P.; Bouscasse, L.; Neri, R.; Lopez-Sepulcre, A.; Valdivia-Mena, M.; Maureira, M.; Henning, T.; et al. PRODIGE-Envelope to Disk with NOEMA-II. Small-Scale Temperature Structure and Streamer Feeding the SVS13A Protobinary Based on CH3CN and DCN. *Astron. Astrophys.* **2023**, *669*, No. A137.

(14) Galván-Madrid, R.; Zhang, Q.; Keto, E.; Ho, P. T.; Zapata, L. A.; Rodríguez, L. F.; Pineda, J. E.; Vázquez-Semadeni, E. From the Convergence of Filaments to Disk-Outflow Accretion: Massive Star Formation in W33A. *Astrophys. J.* **2010**, *725*, No. 17.

(15) Ilee, J. D.; Cyganowski, C.; Nazari, P.; Hunter, T.; Brogan, C.; Forgan, D.; Zhang, Q. G11.92−0.61 MM1: A Keplerian Disc Around a Massive Young Proto-O Star. *Mon. Not. R. Astron. Soc.* **2016**, *462*, 4386−4401.

(16) Öberg, K. I.; Guzmán, V. V.; Furuya, K.; Qi, C.; Aikawa, Y.; Andrews, S. M.; Loomis, R.; Wilner, D. J. The Comet-Like Composition of a Protoplanetary Disk As Revealed by Complex Cyanides. *Nature* **2015**, *520*, 198−201.

(17) Bergner, J. B.; Guzmán, V. G.; Öberg, K. I.; Loomis, R. A.; Pegues, J. A Survey of CH_3CN and HC_3N in Protoplanetary Disks. *Astrophys. J.* **2018**, *857*, 69.
(18) Le Gal, R.; Öberg, K. I.; Teague, R.; Loomis, R. A.; Law, C. J.; Walsh, C.; Bergin, E. A.; Ménard, F.; Wilner, D. J.; Andrews, S. M.; et al. Molecules with ALMA at Planet-Forming Scales (MAPS). XII. Inferring the C/O and S/H Ratios in Protoplanetary Disks with Sulfur Molecules. *Astrophys. J., Suppl. Ser.* **2021**, *257*, 12.
(19) Belloche, A.; Menten, K.; Comito, C.; Müller, H.; Schilke, P.; Ott, J.; Thorwirth, S.; Hieret, C. Detection of Amino Acetonitrile in Sgr B2 (N). *Astron. Astrophys.* **2008**, *492*, 769−773.
(20) Danger, G.; Bossa, J.-B.; De Marcellus, P.; Borget, F.; Duvernay, F.; Theulé, P.; Chiavassa, T.; d'Hendecourt, L. Experimental Investigation of Nitrile Formation From VUV Photochemistry of Interstellar Ices Analogs: Acetonitrile and Amino Acetonitrile. *Astron. Astrophys.* **2011**, *525*, No. A30.
(21) Zhang, X.; Quan, D.; Li, X.; Esimbek, J.; Li, F.; Zhou, Y.; Li, D. Chemical Models of Interstellar Glycine and Adenine Precursor Aminoacetonitrile (NH_2CH_2CN). *Mon. Not. R. Astron. Soc.* **2024**, *533*, 3623−3636.
(22) Krohn, O. A.; Lewandowski, H. Cold Ion−Molecule Reactions in the Extreme Environment of a Coulomb Crystal. *J. Phys. Chem. A* **2024**, *128*, 1737−1752.
(23) Krohn, O. A.; Catani, K. J.; Greenberg, J.; Sundar, S. P.; da Silva, G.; Lewandowski, H. J. Isotope-Specific Reactions of Acetonitrile (CH_3CN) With Trapped, Translationally Cold CCl^+. *J. Chem. Phys.* **2021**, *154*, No. 074305.
(24) Krohn, O. A.; Catani, K.; Sundar, S. P.; Greenberg, J.; da Silva, G.; Lewandowski, H. J. Reactions of Acetonitrile with Trapped, Translationally Cold Acetylene Cations. *J. Phys. Chem. A* **2023**, *127*, 5120−5128.
(25) Neufeld, D. A.; Wolfire, M. G. The Chemistry of Interstellar Molecules Containing the Halogen Elements. *Astrophys. J.* **2009**, *706*, 1594.
(26) Muller, S.; Le Gal, R.; Roueff, E.; Black, J.; Faure, A.; Guélin, M.; Omont, A.; Gérin, M.; Combes, F.; Aalto, S. Protonated Acetylene in the z = 0.89 Molecular Absorber Toward PKS 1830−211. *Astron. Astrophys.* **2024**, *683*, No. A62.
(27) Muller, S.; Kawaguchi, K.; Black, J.; Amano, T. Detection of Extragalactic CF^+ Toward PKS 1830−211-Chemical Differentiation in the Absorbing Gas. *Astron. Astrophys.* **2016**, *589*, No. L5.
(28) Muller, S.; Beelen, A.; Guélin, M.; Aalto, S.; Black, J. H.; Combes, F.; Curran, S.; Theule, P.; Longmore, S. Molecules at z = 0.89 - A 4-mm-Rest-Frame Absorption-Line Survey Toward PKS 1830−211. *Astron. Astrophys.* **2011**, *535*, No. A103.
(29) Wallström, S. H. J.; Muller, S.; Roueff, E.; Le Gal, R.; Black, J.; Gérin, M. Chlorine-Bearing Molecules in Molecular Absorbers at Intermediate Redshifts. *Astron. Astrophys.* **2019**, *629*, No. A128.
(30) Marcus, R. A. Unimolecular dissociations and free radical recombination reactions. *J. Chem. Phys.* **1952**, *20*, 359−364.
(31) Kraka, E.; Antonio, J. J.; Freindorf, M. Reaction mechanism - explored with the unified reaction valley approach. *Chem. Commun.* **2023**, *59*, 7151−7290.
(32) Kraka, E.; Zou, W.; Tao, Y.; Freindorf, M. Exploring the Mechanism of Catalysis with the Unified Reaction Valley Approach (URVA) - A Review. *Catalysts* **2020**, *10*, 691.
(33) Nanayakkara, S.; Kraka, E. A New Way of Studying Chemical Reactions: A Hand-in-hand URVA and QTAIM Approach. *Phys. Chem. Chem. Phys.* **2019**, *21*, 15007−15018.
(34) Freindorf, M.; Beiranvand, N.; Delgado, A. A. A.; Tao, Y.; Kraka, E. On the formation of CN bonds in Titan's atmosphere − a Unified Reaction Valley Approach study. *J. Mol. Model.* **2021**, *27*, No. 320.
(35) Nixon, C. A. The Composition and Chemistry Titan's Atmosphere. *ACS Earth Space Chem.* **2024**, *8*, 406−456.
(36) Hörst, S. M. Titan's Atmosphere and Climate. *J. Geophys. Res.: Planets* **2017**, *122*, 432−482.
(37) Abplanalp, M. J.; Frigge, R.; Kaiser, R. I. Low-Temperature Synthesis of Polycyclic Aromatic Hydrocarbons in Titan's Surface Ices and on Airless Bodies. *Sci. Adv.* **2019**, *5*, No. eaaw5841.
(38) Zhou, L.; Zheng, W.; Kaiser, R. I.; Landera, A.; Mebel, A. M.; Liang, M.-C.; Yung, Y. L. Cosmic-Ray-Mediated Formation of Benzene on the Surface of Saturn's Moon Titan. *Astrophys. J.* **2010**, *718*, 1243.
(39) Kraka, E. Reaction Path Hamiltonian and the Unified Reaction Valley Approach. *Wiley Interdiscip. Rev.: Comput. Mol. Sci.* **2011**, *1*, 531−556.
(40) Kraka, E.; Cremer, D. Computational Analysis of the Mechanism of Chemical Reactions in Terms of Reaction Phases: Hidden Intermediates and Hidden Transition States. *Acc. Chem. Res.* **2010**, *43*, 591−601.
(41) Cremer, D.; Kraka, E. From Molecular Vibrations to Bonding, Chemical Reactions, and Reaction Mechanism. *Curr. Org. Chem.* **2010**, *14*, 1524−1560.
(42) Zou, W.; Sexton, T.; Kraka, E.; Freindorf, M.; Cremer, D. A New Method for Describing the Mechanism of a Chemical Reaction Based on the Unified Reaction Valley Approach. *J. Chem. Theory Comput.* **2016**, *12*, 650−663.
(43) Cremer, D.; Pople, J. A. General Definition of Ring Puckering Coordinates. *J. Am. Chem. Soc.* **1975**, *97*, 1354−1358.
(44) Head-Gordon, M.; Pople, J. A.; Frisch, M. J. MP2 Energy Evaluation by Direct Methods. *Chem. Phys. Lett.* **1988**, *153*, 503−506.
(45) Møller, C.; Plesset, M. S. Note on an approximate treatment for many-electron systems. *Phys. Rev.* **1934**, *46*, 618−622.
(46) Dunning, T. H. Gaussian Basis Sets for Use in Correlated Molecular Calculations. I. The Atoms Boron Through Neon and Hydrogen. *J. Chem. Phys.* **1989**, *90*, 1007−1023.
(47) Woon, D. E.; Dunning, T. H. Gaussian Basis Sets for Use in Correlated Molecular Calculations. III. The Atoms Aluminum Through Argon. *J. Chem. Phys.* **1993**, *98*, 1358−1371.
(48) Zhao, Y.; Truhlar, D. G. Density Functionals with Broad Applicability in Chemistry. *Acc. Chem. Res.* **2008**, *41*, 157−167.
(49) Kendall, R. A.; Dunning, T. H.; Harrison, R. J. Electron Affinities of the First-Row Atoms Revisited. Systematic Basis Sets and Wave Functions. *J. Chem. Phys.* **1992**, *96*, 6796−6806.
(50) Riplinger, C.; Neese, F. An Efficient and Near Linear Scaling Pair Natural Orbital Based Local Coupled Cluster Method. *J. Chem. Phys.* **2013**, *138*, No. 034106.
(51) Neese, F. Software Update: The ORCA Program System—Version 5.0. *Wiley Interdiscip. Rev.: Comput. Mol. Sci.* **2022**, *12*, No. e1606.
(52) Luchini, G.; Alegre-Requena, J. V.; Funes-Ardoiz, I.; Paton, R. S. GoodVibes: Automated Thermochemistry for Heterogeneous Computational Chemistry Data. *F1000Research* **2020**, *9*, 291.
(53) Araki, M.; Takano, S.; Kuze, N.; Minami, Y.; Oyama, T.; Kamegai, K.; Sumiyoshi, Y.; Tsukiyama, K. Observations and Analysis of Absorption Lines Including J = K Rotational Levels of CH_3CN: The Envelope of Sagittarius B2(M). *Mon. Not. R. Astron. Soc.* **2020**, *497*, 1521−1535.
(54) Petrignani, A.; Candian, A. *New Frontiers in Astrobiology*; Thombre, R.; Vaishampayan, P., Eds.; Elsevier, 2022; Chapter 3, pp 49−66.
(55) Fukui, K. The Path of Chemical Reactions - The IRC Approach. *Acc. Chem. Res.* **1981**, *14*, 363−368.
(56) Frisch, M. J.et al. *Gaussian 16*, revision C.01; Gaussian Inc.: Wallingford CT, 2016.
(57) Glendening, E. D.; Badenhoop, J. K.; Reed, A. E.; Carpenter, J. E.; Bohmann, J. A.; Morales, C. M.; Karafiloglou, P.; Landis, C. R.; Weinhold, F. *NBO 7.0*; Theoretical Chemistry Institute; University of Wisconsin: Madison, 2018.
(58) Tao, Y.; Zou, W.; Freindorf, M.; Cremer, D.; Kraka, E. *Computational and Theoretical Chemistry Group (CATCO)*; Southern Methodist University: Dallas, TX, USA, 2021.
(59) Hratchian, H. P.; Kraka, E. Improved Predictor-Corrector Integrators For Evaluating Reaction Path Curvature. *J. Chem. Theory Comput.* **2013**, *9*, 1481−1488.

(60) Lee, T. J.; Schaefer, H. F., III The Classical and Nonclassical Forms of Protonated Acetylene, $C_2H_3^+$. Structures, Vibrational Frequencies, and Infrared Intensities From Explicitly Correlated Wave Functions. *J. Chem. Phys.* **1986**, *85*, 3437−3443.
(61) Lindh, R.; Roos, B. O.; Kraemer, W. P. A CAS SCF CI Study of the Hydrogen Migration Potential in Protonated Acetylene, $C_2H_3^+$. *Chem. Phys. Lett.* **1987**, *139*, 407−416.
(62) Lindh, R.; Rice, J. E.; Lee, T. J. The Energy Separation Between the Classical and Nonclassical Isomers of Protonated Acetylene. An Extensive Study in One-and N-Particle Space. *J. Chem. Phys.* **1991**, *94*, 8008−8014.
(63) Curtiss, L. A.; Pople, J. A. Theoretical Study of Structures and Energies of Acetylene, Ethylene, and Vinyl Radical and Cation. *J. Chem. Phys.* **1988**, *88*, 7405−7409.
(64) Psciuk, B. T.; Benderskii, V. A.; Schlegel, H. B. Protonated Acetylene Revisited. *Theor. Chem. Acc.* **2007**, *118*, 75−80.
(65) Sharma, A. R.; Wu, J.; Braams, B. J.; Carter, S.; Schneider, R.; Shepler, B.; Bowman, J. M. Potential Energy Surface and MULTI-MODE Vibrational Analysis of $C_2H_3^+$. *J. Chem. Phys.* **2006**, *125*, No. 224306.
(66) Crofton, M. W.; Jagod, M.-F.; Rehfuss, B. D.; Oka, T. Infrared Spectroscopy of Carbo-Ions. V. Classical vs Nonclassical Structure of Protonated Acetylene $C_2H_3^+$. *J. Chem. Phys.* **1989**, *91*, 5139−5153.
(67) Gabrys, C. M.; Uy, D.; Jagod, M.-F.; Oka, T.; Amano, T. Infrared Spectroscopy of Carboions. 8. Hollow Cathode Spectroscopy of Protonated Acetylene, C2H3+. *J. Phys. Chem. A* **1995**, *99*, 15611−15623.
(68) Knoll, L.; Vager, Z.; Marx, D. Experimental Versus Simulated Coulomb-Explosion Images of Flexible Molecules: Structure of Protonated Acetylene $C_2H_3^+$. *Phys. Rev. A* **2003**, *67*, No. 022506.
(69) Vager, Z.; Zajfman, D.; Graber, T.; Kanter, E. Experimental evidence for anomalous nuclear delocalization in $C_2H_3^+$. *Phys. Rev. Lett.* **1993**, *71*, 4319.
(70) Cremer, D.; Kraka, E. Theoretical Determination of Molecular Structure and Conformation. 15. Three-Membered Rings: Bent Bonds, Ring Strain, and Surface Delocalization. *J. Am. Chem. Soc.* **1985**, *107*, 3800−3810.
(71) Shi, X.; Li, W.; Schlegel, H. B. Computational Simulations of Hydrogen Circular Migration in Protonated Acetylene Induced by Circularly Polarized Light. *J. Chem. Phys.* **2016**, *145*, No. 084309.
(72) Hough, J.; Bailey, J.; Chrysostomou, A.; Gledhill, T.; Lucas, P.; Tamura, M.; Clark, S.; Yates, J.; Menard, F. Circular Polarisation in Star-Forming Regions: Possible Implications for Homochirality. *Adv. Space Res.* **2001**, *27*, 313−322.
(73) Pentsak, E. O.; Murga, M. S.; Ananikov, V. P. Role of acetylene in the chemical evolution of carbon complexity. *ACS Earth Space Chem.* **2024**, *8*, 798−856.
(74) Turner, B. E. Detection of interstellar cyanoacetylene. *Astrophys. J.* **1971**, *163*, L35.
(75) Johnson, D. R.; Lovas, F.; Gottlieb, C.; Gottlieb, E.; Litvak, M.; Guelin, M.; Thaddeus, P. Detection of interstellar ethyl cyanide. *Astrophys. J.* **1977**, *218*, 370−376.
(76) Belloche, A.; Garrod, R.; Müller, H.; Menten, K.; Comito, C.; Schilke, P. Increased complexity in interstellar chemistry: detection and chemical modeling of ethyl formate and n-propyl cyanide in Sagittarius B2 (N). *Astron. Astrophys.* **2009**, *499*, 215−232.
(77) Neufeld, D. A.; Schilke, P.; Menten, K. M.; Wolfire, M. G.; Black, J. H.; Schuller, F.; Müller, H. S.; Thorwirth, S.; Güsten, R.; Philipp, S. Discovery of interstellar CF+. *Astron. Astrophys.* **2006**, *454*, L37−L40.

https://doi.org/10.1021/acsearthspacechem.5c00083
ACS Earth Space Chem. 2025, 9, 1837−1847